sciendo
Austrian Journal of Earth Sciences | Vienna | 2023 | Volume 116 | 165–179 | DOI: 10.17738/ajes.2023.0010

The metabasites from the Texel Unit (Austroalpine nappe stack): markers of Cretaceous intracontinental subduction and subsequent collision

Peter Tropper[1*], Martina Tribus[1], Hannah Pomella[2], Gerlinde Habler[3]

[1)] Institute of Mineralogy and Petrography, University of Innsbruck, Innrain 52f, A-6020 Innsbruck, Austria. peter.tropper@uibk.ac.at; martina.tribus@uibk.ac.at

[2)] Institute of Geology, University of Innsbruck, Innrain 52f, A-6020 Innsbruck, Austria. hannah.pomella@uibk.ac.at

[3)] Department of Lithospheric Research, University of Vienna, UZA 2, Josef-Holaubek-Platz 2, A-1090 Vienna, Austria. gerlinde.habler@univie.ac.at

[*)] corresponding author: Peter Tropper, peter.tropper@uibk.ac.at

Keywords: eclogites, high-pressure, Texel unit, Eoalpine orogeny, geothermobarometry

Abstract

Eclogites in the Texel Unit (Austroalpine nappe stack; Eastern Alps, South Tyrol, Italy) represent the westernmost outcrops of the E-W striking Eoalpine High-Pressure Belt (EHB). East of the Tauern Window, the EHB forms part of a Cretaceous intracontinental south-dipping subduction/collision zone. The impetus of this contribution is to extend the geothermobarometric data of the eclogites from the EHB using conventional geothermobarometry and multi-equilibrium calculations as well as Zr-in-rutile/titanite geothermometry and to put the *P-T* results of eclogites and amphibolites from the Texel Unit into the geodynamic framework. The investigated samples of this study are from the Spronser- and the Saltaus valleys (S-Tyrol) in the Austroalpine Texel Unit. The Texel Unit is composed mainly of paragneisses with minor intercalations of micaschists, orthogneisses, amphibolites and subordinately eclogites. The amphibolites from the Spronser valley contain the mineral assemblage amphibole + plagioclase + garnet + clinozoisite/epidote + quartz + titanite ± ilmenite ± rutile ± apatite ± calcite. Chemical zoning in plagioclase and amphibole shows two main growth stages: an older *P*-dominated stage (e.g. albite and barroisite cores) and a younger amphibolite-facies stage. The core of the amphiboles shows barroisite composition, the rim can be chemically classified as hornblende, edenite, tschermakite and pargasite. Geothermobarometric calculations with multi-equilibrium geothermobarometry (THERMOCALC v.3.21) yield temperatures of 600–654°C and pressures of 0.98–1.17 GPa for the same samples. The eclogites from the Saltaus valley contain the peak mineral assemblage omphacite + amphibole + garnet + clinozoisite/epidote + muscovite + quartz + titanite ± ilmenite ± rutile. Thermobarometric calculations, were performed in the system CaO-FeO-MgO-Na_2O-Al_2O_3-FeO-SiO_2-H_2O with the assemblage clinopyroxene + garnet + amphibole + clinozoisite/epidote + muscovite + quartz ± H_2O. The calculations involved an H_2O-absent invariant point (mode-1 calculation) as well as two types of *average P-T* mode-2 calculations. The obtained *average P-T* H2O-absent mode 1 *P-T* conditions are 1.89 ± 0.18 GPa and 578 ± 60°C. Using the *average P-T* mode-2 two types of calculations were done: (1) calculations without amphiboles but with H_2O present, which yield mean *P-T* conditions of 1.95 ± 0.28 GPa and 601 ± 55°C and (2) calculations with amphiboles but without H_2O, which yield mean *P-T* conditions of 1.95 ± 0.26 GPa and 666 ± 77°C. Calculations using THERMOCALC v.3.33 yield similar results with slightly higher pressures of 0.3 GPa. Based on the present geothermobarometric data in conjunction with available mineral ages the eclogites represent the Eoalpine intracontinental subduction stage whereas the amphibolites reflect the subsequent, *P*-accentuated stage of decompression associated with the subsequent Eoalpine collisional stage.

1. Introduction

The Alps are the result of two orogenic cycles, a Cretaceous followed by a Tertiary one (e.g. Froitzheim et al., 1994, 1997; Schmid et al., 2004). This dichotomy is reflected by the distribution of the Alpine tectonometamorphic ages as shown by Oberhänsli et al. (2004). The metamorphism in the Western Alps is predominantly related to the Paleogene event (Neoalpine, in the eastern Alps often referred to as "Tauern event"), more precisely the subduction of the Alpine Tethys whereas Alpine metamorphism of the Austroalpine nappes is of Cretaceous age (Eoalpine) and related to the subduction of the Meliata ocean and related oceanic troughs (Schmid et al., 2004). In the course of the latter event, the Austroalpine Mesozoic cover nappes were largely detached and stacked in a transpressional top-NW regime (Eisbacher et al., 1990) while the subducted basement units from the lower plate underwent a metamorphic overprint up to eclogite-facies conditions in the most internal parts. Regarding the Eoalpine orogeny these high-pressure rocks represent a key feature of the eastern Alpine arc, the E-W striking „Eoalpine High Pressure Belt" (EHB), first named by Thöni and Jagoutz (1993). Schmid et al. (2004) summarised the units related to the EHB under the term Koralpe-Wölz high-pressure nappe system. The EHB extends ~375 km in WSW-ENE-direction from the Texel- and Schneeberg Units in the west, to the Pohorje Mountains in the east (Fig. 1). The EHB is generally interpreted as intracontinental high-pressure shear zone (Schmid et al., 2004; Sölva et al., 2005; Krenn et al., 2011; Pomella et al., 2016), oceanic crust was involved only further east.

Available geochronological data constrain the age of high-pressure metamorphism in the Koralpe-Wölz nappe system based on data obtained from highly-retentive isotopic systems (e.g. U-Pb, Sm-Nd and Lu-Hf), which give a time span for peak pressures at ca. 100–80 Ma (Habler et al., 2006; Thöni, 2006; Miller et al., 2005, Sölva et al., 2005; Zanchetta et al., 2013; Miladinova et al. 2022; Hauke et al., 2019). Most eclogites of the Koralpe-Wölz nappe system equilibrated at pressure around 1.7–2.2 GPa (e.g. Miller and Thöni, 1997; Miladinova et al., 2022). Apart from the ambiguous *P-T* conditions of 2.65–2.90 GPa and 630–690°C postulated for the Texel Unit by Zanchetta et al. (2013), the only confirmed exceptions are the Koralpe/Saualpe eclogites (Miller et al., 2005; Herg and Stüwe, 2018; Miladinova et al., 2022) and the peridotite lenses in the Pohorje Mountain Unit (Janák et al., 2004; Sassi et al., 2004; Miller et al., 2005; Herg and Stüwe, 2018), for which peak pressures of 2–2.4 GPa and > 2.1 GPa, or even 3–3.1 GPa and 760–825°C respectively, were suggested.

The focus of this petrological and geothermobarometric investigation are amphibolite samples from the Spronser valley (Tribus, 2008) as well as four eclogite samples from the Saltaus valley from the investigations of Habler et al. (2006) (Fig. 1). In our study, mineral analyses from eclogites were obtained only from one sample (HK25600) but published mineral chemical data of three other eclogite samples (87A1401, T1302 and HK10600) from Habler et al. (2006) were used for the geothermobarometric calculations. The impetus of this contribution is to extend the geothermobarometric data of the eclogites from conventional geothermobarometry to multi-equilibrium calculations as well as Zr-in-rutile/titanite geothermometry and to put the *P-T* results of eclogites and amphibolites from the Texel Unit into the geodynamic framework.

1.1 Geological overview

The Austroalpine nappes located immediately east and west of the Tauern Window show a similar evolution in terms of lithology, structure, as well as grade and age of metamorphism. Tectonostratigraphically from bottom to top these are the Texel-, Schneeberg- and Ötztal Units west of the Tauern Window, and the Millstatt, Radenthein and Bundschuh Units east of the Tauern Window (Schmid et al., 2004; Krenn et al., 2011). These nappes are considered as part of the Upper Austroalpine basement nappes after Schmid et al. (2004) and as the Lower Central Austroalpine nappes in the terminology of Janak et al. (2004). According to Schmid et al. (2004) the Texel- and Schneeberg Units as well as Millstatt- and Radenthein Units are part of the Koralpe-Wölz high-pressure nappe system.

To the south, these units are tectonically delimited by a fault system known as the 'Southern border of Alpine metamorphism' (SAM, Hoinkes et al., 1999). This tectonic structure is attributed to post-Eoalpine, latest Cretaceous to Paleogene extension (Froitzheim et al., 1994; Fügenschuh, 1995). Some particular faults of the SAM were reactivated during Neoalpine convergence and partially overturned and crosscut during Miocene indentation (Mancktelow et al., 2001; Viola et al., 2001; Pomella et al., 2016).

The eclogites of the Eoalpine High Pressure Belt represent the remnants of intracontinental subduction of crustal materials in an intracontinental shear zone (Schmid et al., 2004). The NW-SE directed change in peak pressure of Eoalpine metamorphism across the Eastern Alps can be observed in the Austroalpine units to the west and the east of the Tauern Window (e.g. Hoinkes et al., 1999; Pomella et al., 2016; Herg and Stüwe, 2018; Klug and Froitzheim, 2022) and has been interpreted to reflect a south- to eastward-dipping subduction (e.g. Janák et al., 2004).

The tectonic interpretation of the metamorphic history of the Austroalpine Units west of the Tauern Window is still under discussion. Pomella et al. (2016) presented a tectonic model solving some problems as the apparently opposing Eoalpine extrusion-directions east and west of the Tauern Window and the contradictory kinematics of the Eoalpine nappe boundaries (in their present spatial position) in the wider Ötztal area. The latter is evident for example in the contemporaneous top W transpressive movement along the N-dipping Vinschgau shear zone (Fig. 1) (Trupchun Phase, ca. 100–80 Ma; Froitzheim et al., 1997) and top-NW normal faulting at the NW-dipping

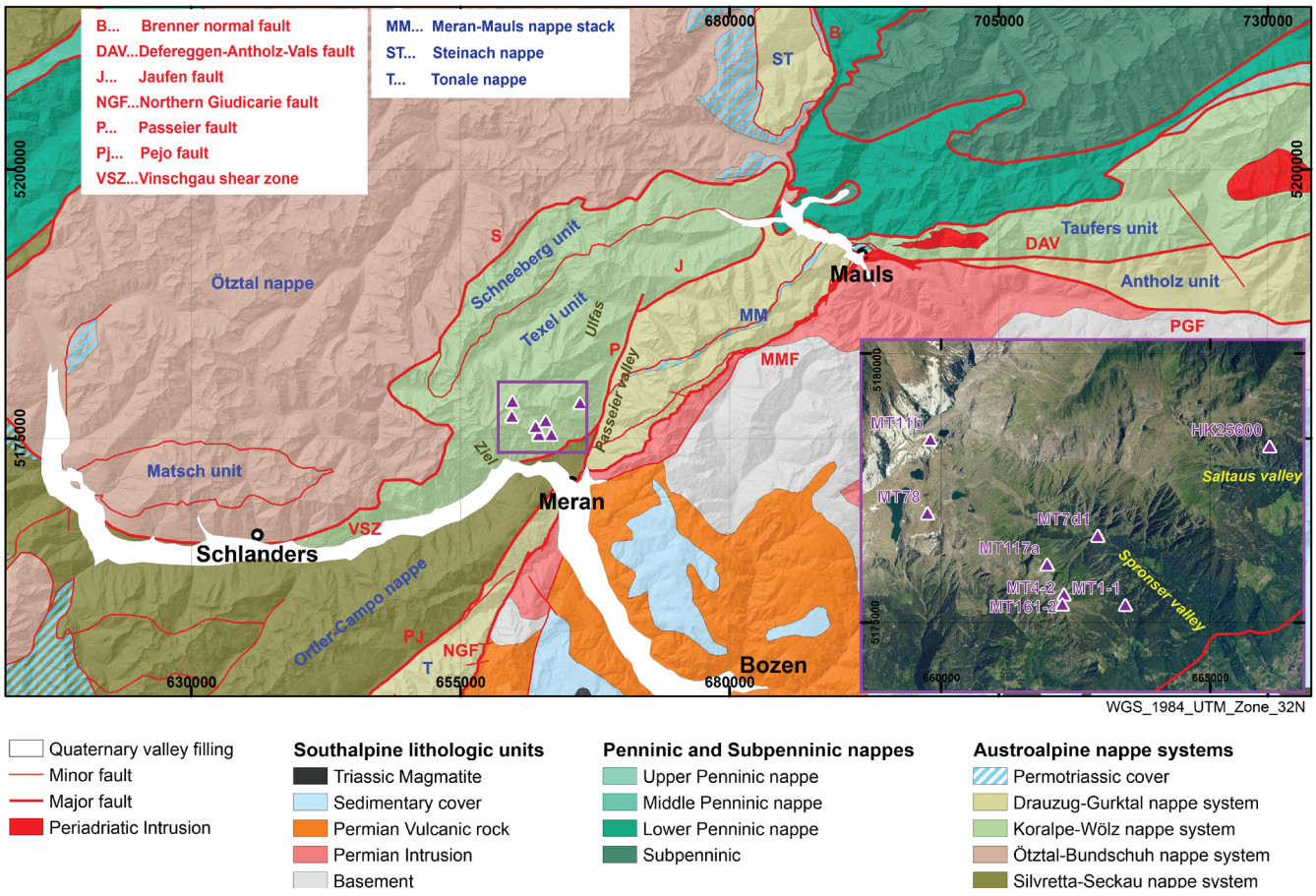

Figure 1: Geological overview of the Austroalpine nappes west of the Tauern Window (updated from Pomella et al. (2022) with data from Montemagni et al. (2023), http://geokatalog.buergernetz.bz.it, and own data); The inset gives a geographical overview of the sample locations. The names of the valleys are given in italics (yellow in the Inlay, green in the main map).

Schneeberg Normal Fault Zone (95–76 Ma; Sölva et al., 2005) without compensational structures in between, as well as the top-SE normal faulting along the SE-dipping Pejo fault and contemporaneous top-SE thrusting along the NW-dipping Jaufen fault (Late Cretaceous; Viola et al., 2003). Pomella et al. (2016) proposed a SSE directed Eoalpine subduction along an intracontinental shear zone east and west of the Tauern Window followed by top-NW directed extrusion of the high pressure units. The so formed nappe stack is cross cut by top-E-SE normal faults related to Late Cretaceous extension (Ducan Ela Phase after Froitzheim et al., 1994). During the Neoalpine orogeny Austroalpine units located in front of the NNW-tip of the Dolomites Indenter experienced a higher degree of shortening than Austroalpine units adjacent to the strike slip Giudicarie fault system or Pustertal-Gailtal fault (Klotz et al., 2019). This resulted in folding (e.g. Vinschgau Shear zone and Schneeberg normal fault) and eventually even overturning (e.g. Jaufen fault) of the nappe stack in front of the Dolomites Indenter, leading to the apparently opposing directions with respect to comparable sections of the EHB further to the east. This model also explains the geometry of the tilted Eoalpine isograds within the Ötztal Unit: After their formation in a ramp position during the Late Cretaceous/Early Tertiary, they were tilted by subsequent Oligocene-Miocene indentation and uplift of the eastern part of the Ötztal Unit.

Klug and Froitzheim (2022) present a quite different geometrical interpretation of the nappe stack west of the Tauern Window. Based on microprobe mapping of garnet and structural field work they concluded the existence of one coherent Ötztal Nappe, including the Texel Complex, and accounting the southeastward increase of Eoalpine metamorphism to southeast-directed subduction. This model negates a major tectonic contact between the Ötztal Nappe and the Texel Complex and emphasizes the existence of a unified Ötztal Nappe with an Eoalpine high-pressure part. Additionally, they interpret the Schneeberg unit as Paleozoic sediments with only low-grade (sub-garnet-grade) Variscan metamorphism, which was thrust over the other units and their Mesozoic cover (Brenner Mesozoic) during an early stage of the Eoalpine orogeny, before the peak of Eoalpine metamorphism and associated garnet growth.

The Texel Unit experienced a polymetamorphic evolution (e.g. Hoinkes et al., 1999; Sölva et al., 2001) with a Variscan imprint reaching amphibolite-facies conditions and a dominant amphibolite-facies overprint of Eoalpine

age. It consists mostly of garnet ± staurolite ± kyanite gneisses with minor amphibolites and marbles (Bargossi et al., 2010). Eclogites are partly intercalated in garnet amphibolites in several localities, e.g. Saltaus (Hoinkes et al., 1991; Miladinova et al., 2022), Moos (Poli, 1991) Sankt Martin (Bargossi et al., 2010) and Ulfas (Zanchetta et al., 2013). Concerning the *P-T* data of the eclogites Hoinkes et al. (1991) initially obtained minimum pressures of 1.1 to 1.2 GPa. Habler et al. (2006) obtained slightly higher pressures of 1.2 to 1.4 GPa. Tribus et al. (2008) calculated *P-T* conditions of 1.8–2.2 GPa and 560–600°C. These data were later confirmed by Miladinova et al. (2022) who obtained *P-T* conditions of 570–600°C and 1.9–2.1 GPa. Zanchetta et al. (2013) determined *P-T* conditions of eclogites from the Texel Unit at UHP conditions of 2.65–2.90 GPa and 630–690°C. Garnet Sm-Nd data (Habler et al., 2006) and zircon U-Pb data (Zanchetta et al., 2013) constrain the age of Eoalpine eclogite-facies metamorphism at 85 ± 5 Ma. Garnet amphibolites containing diopside + plagioclase ± amphibole symplectites are widespread throughout the Texel Unit. These reaction features developed during decompression to *P*-accentuated amphibolite-facies conditions which reached ca. 580–660°C and 0.9–1.2 GPa (Poli, 1991; Spalla, 1993; Zanchetta et al., 2013; Pomella et al., 2016).

The aim of this contribution is to extend the geothermobarometric data of the westernmost metabasites from the EHB (amphibolites and eclogites) of the Texel Unit and to put the *P-T* results of the eclogites and amphibolites into the existing geodynamic framework.

2. Analytical methods

Electron-probe microanalysis (EPMA) was done using the JEOL 8100 SUPERPROBE at the Institute of Mineralogy and Petrography at the University of Innsbruck. Analytical conditions were 15 kV and 10 nA sample current. Counting times for the point measurements were 20 s on the peak and 10 s on the backgrounds. The following standards (standardized element in parenthesis) were used: jadeite (Na), orthoclase (K, Si), rutile (Ti), rhodonite (Mn), diopside (Ca, Mg), chromite (Cr), almandine (Fe), and corundum (Al).

3. Petrography

A total of eight amphibolite samples (MT1-1, MT78, MT161-2; MT117a, MT7d1, MT4-2, MT265a, MT11b) from the Spronser valley and one eclogite sample (HK25600) from the Saltaus valley were investigated with respect to their petrography and mineral chemistry (Fig. 1).

3.1 Amphibolites

The samples examined from the Spronser valley contain the following mineral assemblage: amphibole + plagioclase + garnet + clinozoisite/epidote + titanite + quartz (Fig. 2a). The following minerals occur as accessories: calcite + ilmenite + rutile + apatite + zircon. The amphibolites show a grano- to porphyroblastic structure. Up to 4 mm sized garnet porphyroblasts, host mineral inclusions of amphibole, plagioclase, epidote, titanite, and quartz.

3.2 Eclogites

The four eclogite samples (the data of three of them, 87A1401, HK1060, T1302 are given in Habler et al. (2006)) contain the following mineral assemblage: omphacite + amphibole + garnet + clinozoisite/epidote + quartz + rutile + titanite (Fig. 2b). Figure 2c-d illustrate the various growth-related microstructures of clinopyroxene and amphibole. In the investigated sample HK25600 of this study five different types of clinopyroxenes (A-E) can be distinguished based on microstructural features, composition, compositional zoning, and the particular microdomain (Fig. 2c,d): compositionally homogeneous omphacites (Type A); symplectitic clinopyroxenes (Type B); clinopyroxenes with compositional zoning adjacent to garnet (Type C); clinopyroxenes showing transformation into amphibole (Type D); clinopyroxenes with amphibole inclusions (Type E). In addition, four different amphibole types can be distinguished (indicated with a-d in Fig. 2c): weakly zoned matrix amphiboles with partially idiomorphic morphology (Type a), amphiboles which formed from clinopyroxene (Type b), amphiboles which occur as inclusions in clinopyroxene (Type c) and amphiboles as breakdown product of garnet (Type d). These amphiboles show a high chemical variability. In contrast to Habler et al. (2006), who described albite inclusions in omphacite, the coexistence of plagioclase and omphacite could not be observed in this sample. This has profound implications for geothermobarometry as outlined below.

4. Mineral chemistry

4.1 Amphibolites

Amphiboles: In all samples core and rim domains of amphibole differ in major element composition (Fig. 2e, Tab. 1). While the cores are barroisites (Na-Ca amphiboles, c in Fig. 2c), the compositions of rim domains vary between edenite, pargasite and tschermakite (Ca-amphiboles) as shown in Figure 3a. The Ca amphiboles are chemically zoned, which is mainly based on variations of Al[T], Na[B] and Mg[C]. Therefore, the amphibole rims can be divided into an outer rim R2 (pargasite) and an inner rim R1 (tschermakite) as shown in Figure 2e. In some domains, an outermost rim (R3) occurs, which is composed of magnesio-hornblendes. Plotting Na[B] vs. Al[C] for amphibole analyses from core and rim (R1+R2 and R3) shows decreasing glaucophane component from the core to the rims (Fig. 3b). Furthermore, increasing edenite component occurs from core to rim (Fig. 3c).

Plagioclase: Matrix plagioclase often shows discontinuous zoning and can be divided into a core (C), an inner rim (R1) and an outer rim (R2) as shown in Figure 2f. The

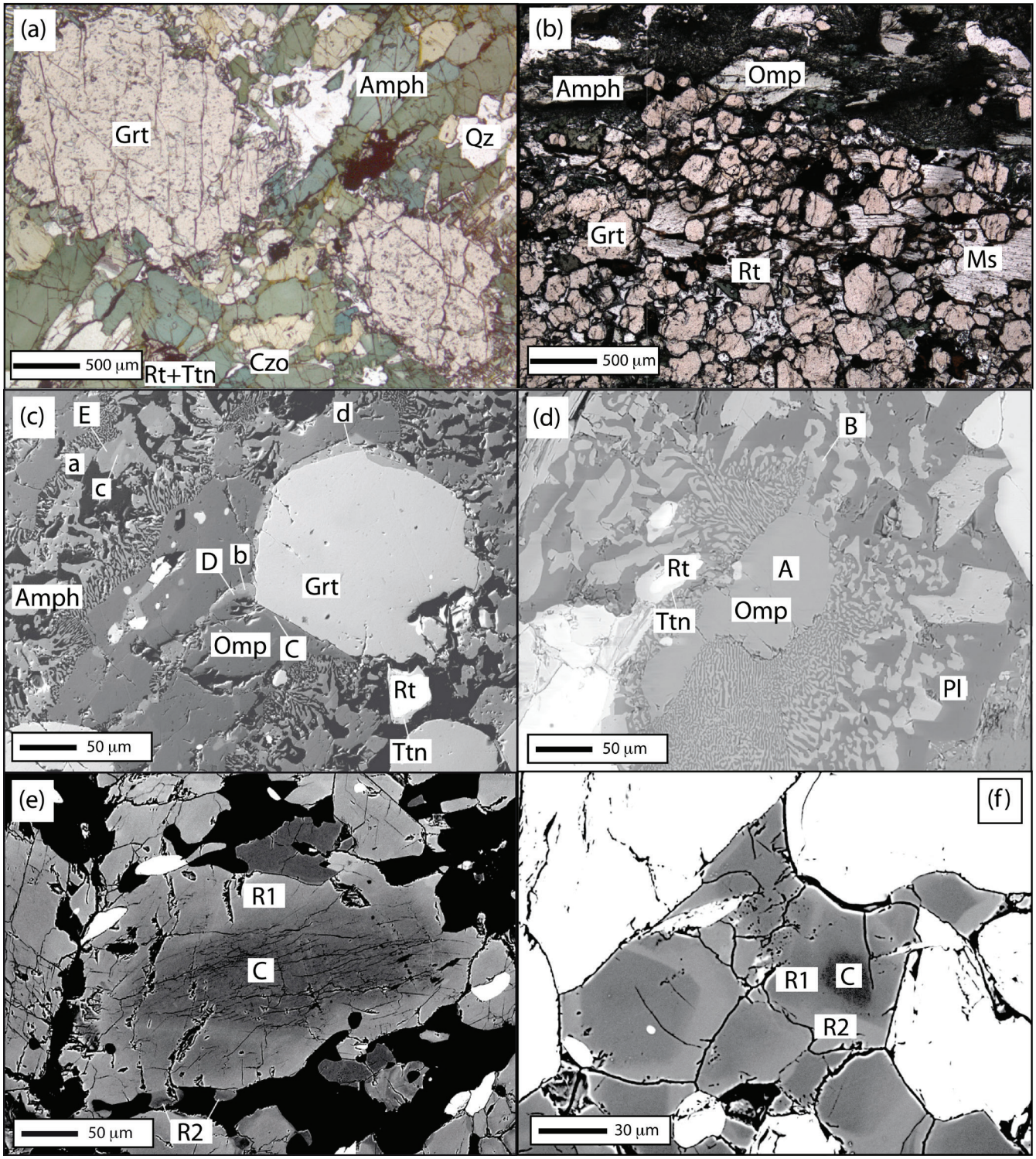

Figure 2: Textures of amphibolite and eclogite samples. (a) Microphotograph of garnet-amphibolite sample MT117a. Reaction rims around garnets are constituted by Al-rich hornblendes. (b) Microphotograph of eclogite sample HK25600a. The fine-grained dark areas are symplectites composed of albite + Na-bearing diopside. (c), (d) Backscatter electron (BSE) images of eclogite sample HK25600 illustrating the different types of clinopyroxene (type indicated with capital letters A–E) and amphibole (type indicated with small letters a-d). (c) clinopyroxene (microstructurally distinct Types A–E as described in the text) and (d) amphibole (microstructurally distinct types a-d as described in the text). Abbreviations: Grt = garnet; Amph = amphibole; Czo = clinozoisite; Rt+Ttn = rutile/titanite intergrowth; Qz = quartz; Omp = omphacite; Rt = rutile; Ms = muscovite; Pl = plagioclase. (e) BSE image of a zoned amphibole porphyroblast in sample MT117. C = core; R1 = inner rim; R2 = outer rim. (f) BSE image showing plagioclase compositional zoning. C = core; R1 = inner rim; R2 = outer rim.

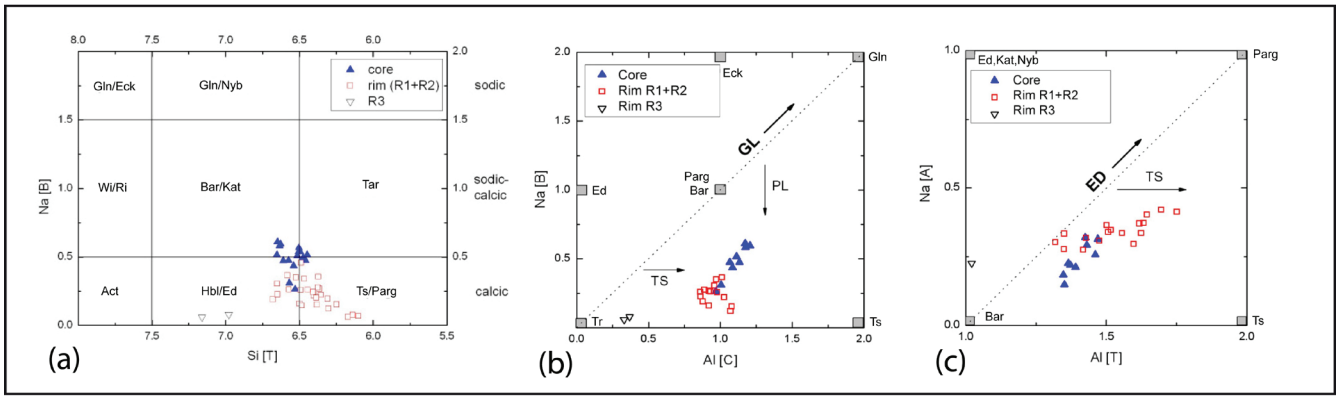

Figure 3: Compositional variations of amphiboles (a-c) in sample MT117. (a) Na[B] vs. Si[T] diagram according to Hawthorn et al. (2012) showing the cores (blue triangles) to be barroisites and the rims (R1 + R2 open red squares, R3 open black triangles) mostly pargasites; (b) Na[B] vs. Al[C] diagram shows decreasing glaucophane (GL) and increasing plagioclase (PL) vectors from core to rim indicating slightly higher *P* conditions in the cores than in the rims; (c) Na[A] vs. Al[T] diagram shows increasing edenite (ED) component from core to rim indicating slightly higher *T* conditions in the rims. There, Tschermaks substitution (TS) also varies strongly. Abbreviations: Gln = glaucophane; Eck = eckerite; Ed = edenite; Parg = pargasite; Bar = barroisite; Tr = tremolite; Ts = tschermakite; Kat = katophorite; Nyb = nyböite; Wi = winchite; Ri = richterite; Tar = taramite; Act = actinolite; Hbl = hornblende.

	Amphibole MT117a				Plagioclase	MT117a		Garnet	MT161-2		Epidote	MT117a			Titanite	MT117a
	R1	R2	R3	core	C	R1	R2	inner core C1	outer core C2	rim	C1	C2	R1	R2		
SiO_2	44.32	41.46	48.44	45.74	67.12	63.88	62.09	39.41	38.78	39.44	38.85	38.21	38.79	38.40	30.99	31.43
TiO_2	0.62	0.74	0.47	0.70	n.d.	n.d.	0.01	0.09	0.12	0.05	0.08	0.03	0.12	0.14	37.80	38.30
Al_2O_3	14.09	16.45	8.18	15.09	21.08	23.42	24.14	21.06	20.93	21.17	28.52	26.89	28.15	28.14	1.41	0.97
Cr_2O_3	n.d.	0.06	n.d.	n.d.	n.d.	0.03	n.d.	0.07	0.03	n.d.	0.11	0.01	0.08	0.11	0.01	0.04
Fe_2O_3	n.c.	n.c.	n.c.	n.c.	n.c.	0.12	0.16	n.c.	0.16	n.c.	6.96	10.00	8.15	8.00	0.27	0.51
FeO	14.69	16.78	14.16	14.23	0.17	n.d.	n.d.	25.73	25.24	25.51	n.d.	n.d.	n.d.	n.d.	n.c.	n.d.
MnO	0.12	0.14	0.10	0.10	n.d.	n.d.	0.02	0.95	4.53	2.10	0.08	0.09	0.03	0.04	n.d.	n.d.
MgO	10.99	8.82	13.64	9.55	n.d.	n.d.	n.d.	2.66	2.27	2.89	0.03	0.05	0.11	0.06	0.01	29.53
CaO	10.45	11.84	12.01	8.52	1.85	4.34	5.64	11.98	9.81	10.81	23.74	23.50	22.93	23.44	29.13	n.d.
Na_2O	2.12	1.86	1.09	2.90	10.79	9.39	8.70	n.d.	n.d.	0.02	n.d.	n.d.	n.d.	n.d.	0.03	n.d.
K_2O	0.53	0.62	0.21	0.57	0.04	0.05	0.04	< 0.01	0.01	0.01	n.d.	n.d.	0.02	0.01	n.d.	0.07
F	n.d.	n.d.	n.d.	n.d.	n.d.	n.d.	n.d.	n.d.	n.d.	n.d.	n.d.	n.d.	n.d.	n.d.	0.13	0.20
F,Cl = O	n.c.	n.c.	n.c.	n.c.	n.c.	n.c.	n.c.	n.c.	n.c.	n.c.	n.c.	n.c.	n.c.	n.c.	0.05	0.03
Total	97.93	98.77	98.30	97.40	101.04	101.22	100.80	101.95	101.88	102.00	98.99	98.79	98.38	98.36	99.94	101.02
															1.005	1.009
Si	6.444	6.102	6.979	6.628	2.917	2.789	2.732	3.046	3.026	3.049	3.001	2.973	3.001	2.978	0.921	0.925
Ti	1.556	1.898	1.021	1.372	n.d.	n.d.	< 0.001	0.005	0.007	0.003	0.005	0.002	0.007	0.008	0.054	0.037
Al	0.859	0.956	0.368	1.205	1.079	1.205	1.252	1.918	1.925	1.928	2.596	2.465	2.566	2.572	< 0.001	0.001
Cr	0.068	0.082	0.051	0.076	n.d.	0.001	n.d.	0.004	0.002	n.d.	0.007	0.001	0.005	0.007	0.007	0.012
Fe^{3+}	0.389	0.262	0.366	0.285	n.c.	0.004	0.005	n.c.	0.009	n.c.	0.405	0.586	0.474	0.467	n.c.	n.d.
Fe^{2+}	1.302	1.758	1.285	1.371	0.006	n.d.	n.d.	1.664	1.647	1.650	n.d.	n.d.	n.d.	n.d.	n.c.	n.c.
Mn	2.382	1.935	2.930	2.063	n.d.	n.d.	0.001	0.063	0.300	0.138	0.005	0.005	0.002	0.003	n.d.	n.d.
Mg	1.628	1.867	1.854	1.323	n.d.	n.d.	n.d.	0.307	0.264	0.333	0.004	0.005	0.013	0.008	0.001	1.016
Ca	0.262	0.069	0.079	0.595	0.086	0.203	0.266	0.993	0.820	0.896	1.965	1.959	1.901	1.948	1.011	n.d.
Na	0.336	0.462	0.226	0.220	0.909	0.795	0.742	n.d.	n.d.	0.003	n.d.	n.d.	n.d.	n.d.	0.002	n.d.
K	0.098	0.116	0.038	0.325	0.002	0.003	0.002	n.d.	0.001	0.001	n.d.	n.d.	0.002	0.001	n.d.	0.008
F	n.d.	n.d.	n.d.	n.d.	n.d.	n.d.	n.d.	n.d.	n.d.	n.d.	n.d.	n.d.	n.d.	n.d.	0.013	0.042
Name	Tschermakite	Pargasite	Mg-Hornblende	Al-Barroisite												
				*X*An	0.086	0.203	0.263									
				*X*Ab	0.911	0.795	0.735									
				*X*Kfs	0.002	0.003	0.002									
							*X*Grs	0.323	0.261	0.295						
							*X*Alm	0.550	0.543	0.546						
							*X*Prp	0.101	0.087	0.110						
							*X*Sps	0.021	0.099	0.046						
										*X*Czo	0.608	0.441	0.578	0.565		
										*X*Ep	0.392	0.559	0.422	0.435		
														*X*Ti	0.938	0.948
														*X*Al	0.055	0.039
														*X*Fe	0.007	0.013
														XO1	0.938	0.950

Table 1: Representative electron probe microanalyses of amphibole, plagioclase, garnet, epidote and titanite from the amphibolites. Amphibole: Formula calculation was done using the program AMPH-IMA 2004 (Mogessie et al., 2001) on the basis of 24 anions and 23 oxygens; n.d. not detected; R1-R3 = rim analyses from innermost rim (R1) to outer rim (R3). Plagioclase: Formulae normalization on the basis of 5 cations and 8 oxygens; n.d. not detected; An = anorthite; Ab = albite; Kfs = K-feldspar; C = core; R1 = inner rim; R2 = outer rim. Garnet: Formula calculation on the basis of 8 cations and 12 oxygens; n.d. not detected; n.c. not calculated; Grs = grossular; Alm = almandine; Prp = pyrope; Sps = spessartine. Epidote: Formula calculation on the basis of 12 oxygens, 1 OH-group; n.d. not detected; Czo = clinozoisite; Ep = epidote; C1 = inner core; C2 = outer core; R1 = inner rim; R2 = outer rim. Titanite: Formulae calculated on the basis of 3 cations; n.d. not detected; *X*O1 = fraction of bridging oxygen.

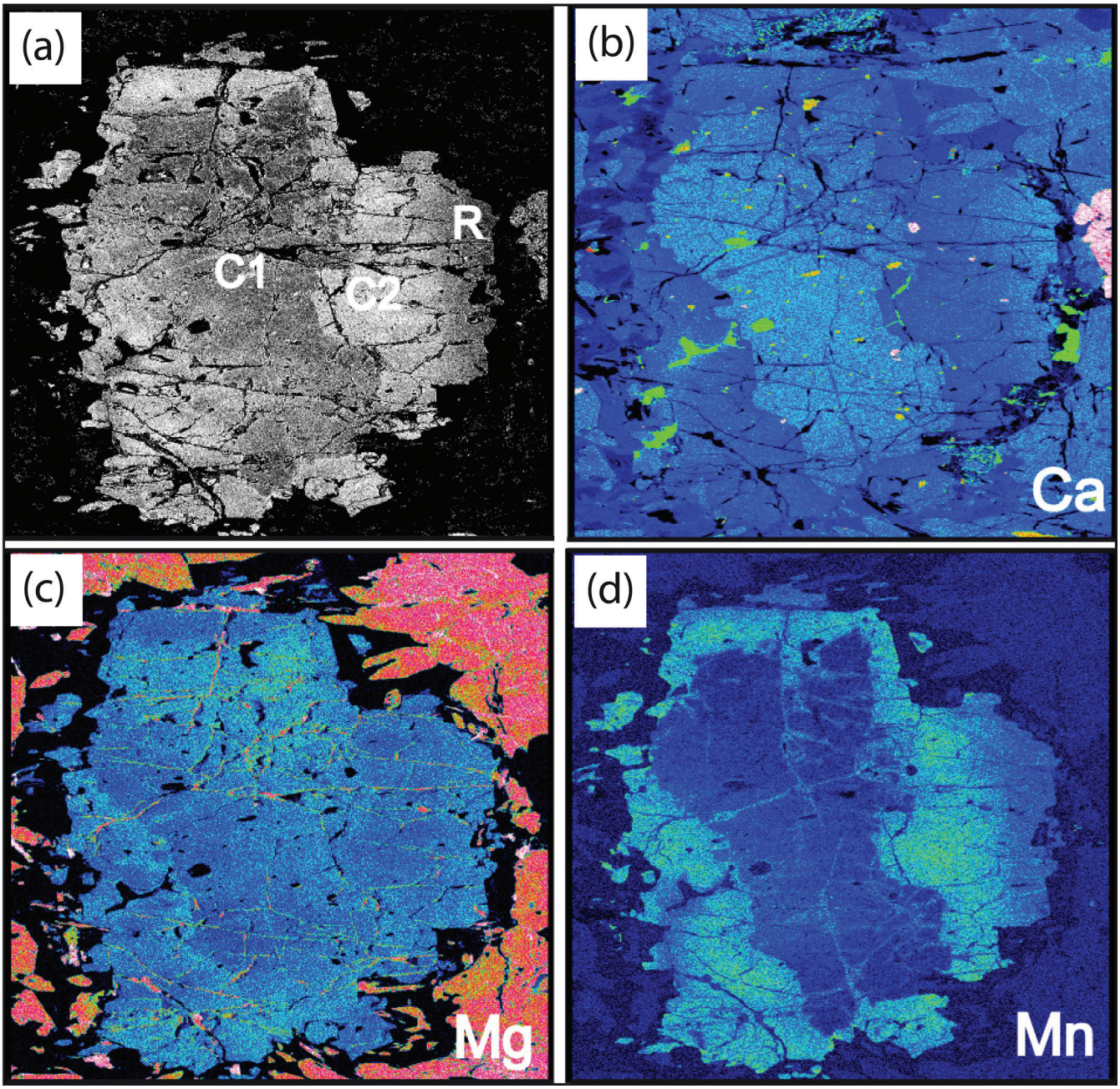

Figure 4: Element distribution of a discontinuously zoned garnet from amphibolite sample MT177; (a) BSE image; C1 = relic core; C2 = inner domain; R = outer rim; (b) Ca distribution; (c) Mg distribution; (d) Mn distribution. Brighter colors in the maps indicate higher element contents.

anorthite content clearly increases from core to the outer rim R2. The average chemical composition of the three zones is: C: Ab_{95-96} An_{4-5}, R1: Ab_{79-87} An_{13-21} and R2: Ab_{66-73} An_{27-34} (Tab. 1).

Garnet: Amphibolite-samples show both discontinuously as well as continuously zoned garnets. In the continuously zoned garnets, chemical zoning is mainly reflected by changes in Mn, Ca and Mg, where Ca and Mg contents increase from core to rim, while Mn and Fe^{2+} reach maximum values in the cores. The core composition $Grs_{29}Alm_{57}Prp_5Sps_8$ changes to $Grs_{32}Alm_{54}Prp_{12}Sps_3$ in the rim. In addition to continuously zoned garnets, discontinuously zoned garnets were observed in all samples (Fig. 4a-d). Surrounding a relic garnet core (C1) garnet further crystallized forming an inner domain (C2) and an outer rim zone (R, Fig. 4a). The boundary between C1 and C2 is reflected by a characteristic decrease in Ca (Fig. 4b) and an increase in Mn (Fig. 4d). The Mg distribution is rather homogeneous (Fig. 4c). Towards the outer rims the Ca content increases again (Fig. 4b). The average garnet compositions are (Tab. 1): Core C1: Grs_{31} Alm_{55} Prp_{10} Sps_2; C2: Grs_{25} Alm_{54} Prp_9 Sps_{10}; rim (R): Grs_{29} Alm_{54} Prp_{11} Sps_5.

Epidotes: The epidote [X_{Ep} = $Fe^{3+}/(Fe^{3+}+Al+Cr-2)$] content varies between 0.39–0.57 (Tab. 1). Although com-

	Amphibole				Garnet		Omphacite					Muscovite	Epidote
Type	a	b	c	d	rim	core	A	B	C	D	E		
SiO_2	43.12	43.02	43.14	37.51	38.57	38.35	54.34	43.04	55.30	56.71	54.18	48.69	38.79
TiO_2	0.93	0.28	0.92	0.16	0.02	0.11	0.19	0.28	0.12	0.11	0.07	0.64	0.18
Al_2O_3	12.44	13.57	12.12	18.29	21.45	21.38	7.81	13.57	9.61	10.58	4.28	29.70	27.21
Cr_2O_3	n.d.	n.d.	n.d.	n.d.	0.01	n.d.	n.d.	< 0.01	n.d.	n.d.	0.04	n.d.	n.d.
Fe_2O_3	n.c.	n.c.	n.c.	n.c.	n.c.	n.c.	5.19	14.90	3.87	2.73	5.54	n.d.	7.59
FeO	17.12	17.48	16.67	19.54	26.02	25.22	3.76	4.08	3.54	3.98	3.39	2.51	n.d.
MnO	0.1	0.15	0.08	0.16	0.42	1.22	0.06	0.15	0.02	n.d.	0.01	0.03	0.02
MgO	9.85	8.85	10.2	7.02	3.58	2.47	8.66	8.85	8.04	7.08	10.78	2.42	0.05
CaO	8.99	9.96	9.06	10.74	9.94	10.92	15.77	9.96	13.88	12.89	19.45	n.d.	23.49
Na_2O	4.08	3.82	4.05	3.55	0.02	n.d.	5.53	3.82	6.59	7.50	3.73	1.32	0.01
K_2O	0.79	0.41	0.83	0.64	n.d.	n.d.	0.01	0.40	n.d.	0.01	n.d.	9.34	n.d.
Total	97.42	97.54	97.07	97.61	100.03	99.68	101.34	99.05	100.98	101.59	101.48	94.65	97.35
Si	6.446	6.441	6.465	5.680	3.024	3.033	1.952	1.953	1.942	1.997	1.962	3.269	3.034
Ti	1.554	1.559	1.535	2.320	0.001	0.006	0.005	0.003	0.004	0.003	0.002	0.032	0.011
Al	0.638	0.836	0.606	0.944	1.982	1.993	0.331	0.299	0.316	0.439	0.183	2.351	2.508
Cr	0.105	0.032	0.104	0.018	0.001	n.d.	n.d.	0.002	n.d.	n.d.	0.001	n.d.	n.d.
Fe^{3+}	0.310	0.176	0.299	0.604	n.c.	n.c.	0.140	0.144	0.165	0.072	0.151	n.c.	0.447
Fe^{2+}	1.752	1.981	1.712	1.849	1.707	1.668	0.113	0.125	0.102	0.117	0.103	0.14	n.c.
Mn	2.195	1.975	2.279	1.585	0.028	0.082	0.002	< 0.001	0.002	n.d.	0.000	0.002	0.001
Mg	1.440	1.598	1.455	1.742	0.419	0.291	0.464	0.495	0.476	0.372	0.582	0.242	0.006
Ca	0.469	0.352	0.457	0.215	0.835	0.926	0.607	0.622	0.619	0.487	0.755	n.d.	1.969
Na	0.714	0.757	0.720	0.827	0.003	n.d.	0.385	0.357	0.373	0.512	0.262	0.172	0.002
K	0.865	0.835	0.879	0.951	n.d.	n.d.	0.001	< 0.001	n.d.	< 0.001	n.d.	0.800	n.d.
	Pargasite	Fe-Pargasite	Pargasite	Fe-Pargasite									
				X Gr	0.278	0.309							
				X Alm	0.571	0.562							
				X Py	0.140	0.098							
				X Sps	0.009	0.028							
						X Aeg	0.140	0.144	0.165	0.072	0.151		
						X Jd	0.245	0.214	0.209	0.440	0.111		
						X Hed	0.111	0.121	0.101	0.117	0.106		
						X Di	0.460	0.478	0.472	0.371	0.596		
											X Pg	0.170	
												X Czo/Zo	0.519
												X Ep	0.447

Table 2: Representative electron probe microanalyses of amphibole, garnet, omphacite, muscovite and epidote from eclogite sample HK25600. Garnet: Formulae calculated on the basis of 8 cations and 12 oxygens; n.d. = not detected; n.c. = not calculated; Grs = grossular; Alm = almandine; Prp = pyrope; Sps = spessartine. Amphibole: Formula calculation was done using the program AMPH-IMA 2004 (Mogessie et al., 2001) on the basis of 24 anions and 23 oxygens; n.d. = not detected; Type a-d = see text. Omphacite: Formulae calculated on the basis of 4 cations and 6 oxygens; n.d. = not detected; n.c. = not calculated; Aeg = aegirine; Jd = jadeite; Hed = hedenbergite; Di = diopside; Type A-E = see text. Muscovite: Formulae calculated on the basis of 11 oxygens; n.d. = not detected; n.c. = not calculated; Pg = paragonite. Epidote: Formulae calculated on the basis of 12 oxygens and 1 OH; n.d. = not detected; n.c. = not calculated.

plex zoning pattern are shown in BSE images, no systematic major element zoning was observed, indicating that compositional zoning is restricted to minor or trace elements.

Accessory minerals: Titanite is the most abundant Ti phase in the studied amphibolite samples. The Al content is low, ranging between 0.03 and 0.05 apfu, with (F + OH) between 0.04 and 0.07 apfu. The Fe^{3+} content varies between 0.006 and 0.012 apfu (Tab. 1).

4.2 Eclogites

Amphibole: According to Habler et al. (2006) amphiboles, which formed in equilibrium with omphacite and occur as inclusions in Grt 2, are magnesiokatophorites - magnesiotaramites or barroisites (Tab. 2). On the other hand, amphibole inclusions in Grt 1 and the cores of the coarse-grained matrix amphiboles are edenites, pargasites and magnesio-hornblendes. In sample HK25600 the amphibole compositions of type c (Fig. 2d) microstructurally correspond to the eclogite facies assemblage of Habler et al. (2006) but are mostly classified as pargasites (Fig. 5).

Garnet: Habler et al. (2006) reported discontinuous chemical zoning in garnet from the Saltaus valley indicating at least two separate garnet growth periods, separated by a stage of Grt decomposition. The authors described an earlier continuously zoned garnet (Grt 1), which was overgrown and enclosed by a later, again continuously zoned garnet (Grt 2). Chemical zoning in both Grt 1 and Grt 2 shows decreasing Ca and Mn contents and increasing Fe and Mg contents from the core

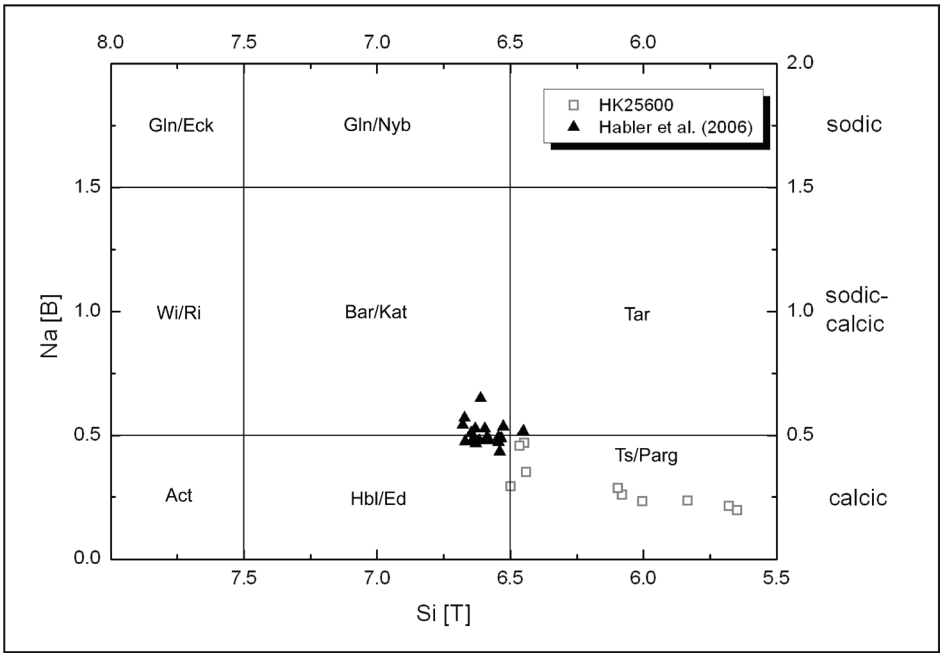

Figure 5: Amphibole composition of eclogite sample HK25600 (open squares) compared to amphibole data from Habler et al. (2006, black triangles) in a Na[B] vs. Si[T] diagram according to Hawthorne et al. (2012). Mineral abbreviations are the same as in Figure 3.

to the rim. The two similarly zoned generations are separated by a Grt zone where Mn is slightly increased. The garnets from sample HK25600 show an irregular zoning pattern with an average composition of Grs_{30} Alm_{57} Prp_{10} Sps_3 (Tab. 2). Towards the rims the Ca and Mn contents decrease slightly (Grs_{28} Sps_1), while the pyrope component increases (Prp_{14}). The Fe^{2+} content is homogeneous throughout garnet.

Clinopyroxene: In the study of Habler et al. (2006) omphacite inclusions in Grt 1 and the cores of the matrix pyroxenes (Omp 1) have lower *X*Jd and Al contents, but higher Fe, Mg and Ca contents than the rims of the matrix omphacites (Omp 2). Accordingly, the clinopyroxenes of the first generation (Omp1) are considered to be equivalent to Amp 1 and thus formed before the pressure maximum, while Omp 2 and Amp 2 were interpreted to represent the pressure peak. The outermost rims of the matrix pyroxenes (Omp 3) show decreasing *X*Jd contents and are therefore assigned to a decompression stage. The clinopyroxenes of types A, C, D and E in sample HK25600 (Fig. 2c,d and Tab. 2) can be classified as omphacites, and clinopyroxene type A corresponds to Omp 2 of Habler et al. (2006). The jadeite content of type A clinopyroxenes varies between 41 and 44 mol.%. In contrast, the symplectitic clinopyroxenes (type B) show high amount of diopside component (X_{Di} = 0.6) and hence low jadeite content of < 11 mol.%. Clinopyroxene types D and E have an average jadeite content of 22 mol%.

Muscovite: White micas are phengitic with Si = 3,27 apfu and a paragonite component of 17% (Tab. 2).

Clinozoisite/epidote: The clinozoisites are weakly zoned, with X_{Fe3+} contents decreasing from the core to the rim from X_{Ep} = 0.5 to 0.45 (Tab. 2).

5. Geothermobarometry

5.1 Amphibolites

For matrix calculations amphibole rim compositions (R1 + R2) coexisting with garnet, plagioclase and quartz were used.

5.1.1 Conventional geothermobarometry

These calculations were carried out using the program PET-Petrological Elementary Tools for Mathematica (Dachs, 1998) and the internally consistent database of Holland and Powell (1998). Geothermometry using the garnet-hornblende Fe-Mg exchange (Dale et al., 2000) yield *T* of 570–650°C for hornblende inclusions and 550–680°C for hornblende coexisting with garnet rims at *P* between 1.2 and 1.4 GPa. Geobarometry using the garnet-hornblende-plagioclase geobarometer according to Dale et al. (2000) yields *P* of 0.9–1.3 GPa for inclusion assemblages and 0.8–1.2 GPa for coexisting rim assemblages at *T* of 600–650°C. The resulting *P-T* conditions are 0.8–1.3 GPa and 570–640°C with no significant differences between core and rim assemblages.

5.1.2 Multi-equilibrium geothermobarometry

Multi equilibrium geothermobarometry was done in the system CaO-FeO-MgO-Na_2O-Al_2O_3-SiO_2-H_2O with the assemblage plagioclase + amphibole + garnet + epidote/clinozoisite + quartz by using the program THERMOCALC v.3.21 (ds55 data set from 2003) coupled with a 2000 version of *AX* to calculate activities and also using THERMOCALC v.3.33 (tcds55s data set from 2009) coupled with a 2008 version of *AX*. The rationale behind this approach of using two versions (v.3.21 and v.3.33) of the same pro-

gram was to test the influence of varying amphibole activities on the *P-T* results. THERMOCALC v.3.21 uses the amphibole activity model of Dale et al. (2000), which was calibrated using naturally occurring hornblende-garnet-plagioclase assemblages while THERMOCALC v.3.33 uses the revised amphibole activity model of Dale et al. (2005) whose calibration is based on naturally coexisting amphibole pairs instead. Two types of calculations were carried out: mode-1 calculations involve an invariant point in the system CaO-FeO-Al_2O_3-SiO_2-H_2O (CFASH). The rationale behind *average P-T* mode-2 calculations is called the *average P-T*-approach, which uses an independent set of reactions from an internally-consistent dataset (Powell and Holland, 2008). Then, the activities of the phase components are calculated from thermodynamic models and the analysed compositions of the phases. This approach considers the activities of each of the end-members of the phases to be variable within their uncertainties and hence each reaction then defines a *P-T* band, the bands being correlated with each other via the activities. The obtained *P-T* conditions are represented by the *P-T* point that is as "close" as possible (in a least-squares sense) to every reaction line. The following invariant point in the system CFASH was used for the mode-1 calculations:

15ferroactinolite + 42clinozoisite = 38grossular + 25almandine + 57quartz + 36H_2O
6ferroactinolite + 21anorthite = 11grossular + 10almandine + 27quartz + 6H_2O
4grossular + 5almandine + 6clinozoisite + 15quartz = 3ferroactinolite + 18anorthite
5almandine + 22clinozoisite + 19quartz = 3 ferroactinolite + 38anorthite + 8H_2O
4clinozoisite + quartz = 5anorthite + grossular + 2H_2O

Mode-1 calculations of mineral inclusion assemblages and hosting garnet yield the following results assuming aH_2O = 1: sample MT 7d1: 556–634°C, 1.08–1.34 GPa and sample MT 117a: 576–645°C, 1.05–1.20 GPa. Furthermore, *average P-T* mode-2 calculations yield 600 ± 56°C, 1.16 ± 0.17 GPa for sample MT 7d1 and 607 ± 44°C, 1.09 ± 0.13 GPa for sample MT 117a.

In order to determine the *P-T* conditions without the influence of water activity (aH_2O) the following H_2O-independent reactions were used for the *average P-T* mode-2 calculations in the system CaO-FeO-MgO-Al_2O_3-SiO_2-H_2O (CFMASH):

3tschermakite + 2pyrope + 4grossular + 12quartz = 3tremolite +12anorthite
15tschermakite + 20grossular + 10almandine + 60quartz = 9tremolite + 12anorthite
3tschermakite + 4grossular + 5almandine + 12quartz = 3ferroactinolite + 12anorthite + 3pyrope
3tremolite + 5almandine = 3ferroactinolite + 5pyrope

Therefrom, the following *P-T* conditions were obtained: sample MT 7d1: 604–617°C, 0.90–1.14 GPa (ΔT = 13°C, ΔP = 0.24 GPa) and sample MT 117a: 605–622°C, 0.75–1.07 GPa (ΔT =17°C, ΔP = 0.32 GPa). The calculations show that the assumption of aH_2O = 1 results in slightly higher pressures (ca. 0.2 GPa) and in a larger spread in temperatures.

Matrix mineral assemblages: Using the H_2O-bearing invariant point described above yield 599–649°C, 0.99–1.07 GPa for sample MT7d1 and 604–648°C, 0.98–1.05GPa for sample MT78. Applying the *average P-T* mode-2 we obtained *P-T* conditions of 617 ± 44°C, 1.05 ± 0.13 GPa for sample MT 7d1: and 609 ± 59°C, 0.98 ± 0.18 GPa for sample MT 78. *Average P-T* calculations in the H_2O-free system yield 654 ± 86°C, 1.11 ± 0.19 GPa for sample MT 7d1, and 633 ± 154°C, 1.06 ± 0.34 GPa for sample MT 78.

Multi-equilibrium geothermobarometry using THERMOCALC *v.3.33:* The study of Guynn et al. (2013) tested THERMOCALC v.3.21 versus THERMOCALC v.3.33 on similar garnet-amphibolites and found out that THERMOCALC v.3.33 clearly calculated much lower pressures than either conventional geothermobarometry or THERMOCALC v.3.21, which was not supported by the mineralogical evidence (e.g. kyanite stability in the coexisting metapelites). This strong shift in pressure is mostly due to lower pargasite and tschermakite and higher tremolite activities emanating from differences in the *AX* program (*AX* 2000 vs. *AX* 2008). Furthermore, the high standard deviations are largely due to slight modifications in the continuously refined thermodynamic data of the internally consistent databases (2003 database ds55 with σ_{fit} = 1.067 v. 2009 database tcds55s with σ_{fit} = 1.202). The calculations of the Texel Unit amphibolites yield an enormous spread in the *P-T* data ranging from 570°C and 1 GPa to 700°C and 1.8 GPa. Although five out of nine calculations yield *P-T* results of 570–680°C and 1–1.1 GPa, the huge 1σ uncertainties associated with these calculations of 80–288°C and 0.13–0.34 GPa make these calculations highly unreliable. Since THERMOCALC v.3.21 uses the Dale et al. (2000) amphibole activity model specifically calibrated for the application to hornblende-garnet-plagioclase geothermobarometry, and the results are well in agreement with conventional geothermobarometry, hence the v.3.21 *P-T* results are regarded as more appropriate.

Zirconium-in-rutile geothermometry using the calibration of Ferry and Watson (2007) yield temperatures of 575–590°C for rutile inclusions in garnet in sample MT11b.

5.2 Eclogite

5.2.1 Multi-equilibrium geothermobarometry

The geothermobarometric calculations, using the program THERMOCALC v. 3.21 were performed in the system CaO-FeO-MgO-Na_2O-Al_2O_3-FeO-SiO_2-H_2O with the assemblage clinopyroxene + garnet + amphibole + clinozoisite/epidote + muscovite + quartz ± H_2O. According to Habler et al. (2006) for the calculations of their samples 87A1401, T1302 and HK10600 only the mineral assem-

THERMOCALC v.3.21

	M1-H_2O-Amph				M2+H_2O-Amph				M2-H_2O+Amph			
	P	1σ	*T*	1σ	*P*	1σ	*T*	1σ	*P*	1σ	*T*	1σ
87A1401_1	1.84	0.18	571	59	1.87	0.34	591	63	1.82	0.27	647	86
87A1401_2	1.85	0.18	570	59	1.86	0.34	582	63	1.83	0.27	652	87
87A1401_3	1.85	0.18	573	59	1.87	0.34	587	62	1.84	0.27	649	86
HK1060_1	2.02	0.17	549	59	2.04	0.30	565	55	2.13	0.25	675	69
HK1060_2	1.89	0.18	607	62	1.88	0.31	590	59	1.94	0.24	671	70
T1302_1	1.82	0.17	570	60	2.11	0.17	612	50	1.99	0.20	675	52
HK25600-1	1.97	0.18	605	64	2.05	0.16	681	32	2.09	0.30	693	90
Mean	**1.89**	**0.18**	**578**	**60**	**1.95**	**0.28**	**601**	**55**	**1.95**	**0.26**	**666**	**77**

THERMOCALC v.3.33

	M1-H_2O-Amph				M2-H_2O-Amph				M2-H_2O+Amph			
	P	1σ	*T*	1σ	*P*	1σ	*T*	1σ	*P*	1σ	*T*	1σ
87A1401_1	2.12	0.18	592	92	2.16	0.28	635	91	2.21	0.22	642	89
87A1401_2	2.34	0.43	647	76	2.17	0.28	625	90	2.19	0.21	628	87
87A1401_3	2.13	0.18	596	93	2.19	0.28	635	90	2.22	0.22	640	88
HK1060_1	2.16	0.17	563	122	2.30	0.26	619	84	2.39	0.20	623	84
HK1060_2	2.02	0.18	622	104	2.06	0.24	626	84	2.34	0.22	669	88
T1302_1	1.79	0.16	576	110	2.29	0.28	651	104	2.31	0.23	652	102
HK25600-1	2.26	0.19	628	116	2.35	0.32	726	101	2.47	0.24	741	71
Mean	**2.12**	**0.21**	**603**	**102**	**2.22**	**0.28**	**645**	**92**	**2.30**	**0.22**	**656**	**87**

Table 3: Calculated *P-T* results of the eclogites using THERMOCALC v.3.21 and v.3.33. M1-H_2O-Amph: mode-1 no H_2O no amphiboles; M2+H_2O-Amph: *Average P-T* mode-2 plus H_2O no amphiboles; M2-H_2O+Amph: *Average P-T* mode-2 no H_2O but with amphiboles; M2-H_2O-Amph: *Average P-T* mode-2 no H_2O no amphiboles; M2-H_2O+Amph: *Average P-T* mode-2 no H_2O but with amphiboles.

blage of phase generation 2 (peak eclogite-facies stage) was used. The calculations of sample HK25600 were done with the growth stage attributions of the phases according to Habler et al. (2006) using the compositions of their amphibole type C, garnet rim and clinopyroxene type A (see section petrography and mineral chemistry of the eclogite). The calculations involved an H_2O-absent invariant point without amphiboles (mode-1 calculation, M1-H_2O-Amp) as well as two types of *average P-T* mode-2 calculations, with H_2O and without amphiboles, M2+H_2O-Amp, and without H_2O and amphiboles, M2-H_2O+Amp) calculations. The following amphibole- and H_2O-absent invariant point in the system K_2O-CaO-FeO-MgO-Al_2O_3-SiO_2-H_2O (KCFMASH) was used for the calculations (M1-H_2O-Amph):

pyrope + 2grossular + 3celadonite = 6diopside + 3muscovite
2grossular + almandine + 3celadonite = 3diopside + 3hedenbergite + 3muscovite
2grossular + 2almandine + 3celadonite = pyrope + 6hedenbergite + 3muscovite
pyrope + 3hedenbergite = almandine + 3diopside

The obtained *average P-T* conditions of the four samples are 1.89 ± 0.18 GPa and 578 ± 60°C (Tab. 3). Using the *average P-T* mode-2 two types of calculations were done: 1.) calculations without amphiboles but with H_2O present (M2+H_2O-Amph):

15diopside + 12clinozoisite = 5pyrope + 13grossular + 12quartz + $6H_2O$
15hedenbergite + 12clinozoisite = 13grossular + 5almandine + 12quartz + $6H_2O$
pyrope + 2grossular + 3celadonite = 6diopside + 3muscovite

This yields *average P-T* conditions of 1.95 ± 0.28 GPa and 601 ± 55°C for the four samples (Tab. 3) and 2.) calculations with amphiboles but without H_2O (M2-H_2O+Amph).

4grossular + 3tschermakite + 3quartz = pyrope + 6diopside + 6clinozoisite
pyrope + 3hedenbergite = almandine + 3diopside
5almandine + 12diopside + 3tschermakite = 7pyrope + 4grossular + 3ferroactinolite
pyrope + 2grossular + 3celadonite = 6diopside + 3muscovite
2pyrope + 4grossular + 3glaucophane = 6diopside + 6jdadeite + 3tschermakite
4pyrope + 12diopside + 3pargasite + 18clinozoisite = 10grossular + 3jdadeite + 12tschermakite

This yields *average P-T* conditions of 1.95 ± 0.26 GPa and 666 ± 77°C using THERMOCALC v.3.21 (Tab. 3). It is also interesting to note that calculations involving amphiboles (M2-H_2O+Amph) show a marked increase in *T* of about 60°C.

When using THERMOCALC v.3.33 the obtained *P-T* re-

sults slightly change with respect to *P* and *T* (Table 3). The amphibole- and H_2O-absent calculations using mode-1 (M1-H_2O-Amph) only change slightly in *T* (ca. 20°C) but yield an increase of 0.2 GPa in *P*. This is mostly due to the addition of the phase component of ferroceladonite to the calculations. This is also visible in the calculations using *average P-T* mode-2 (M2-H_2O-Amph), which show a change in temperature of almost 50°C. This affected the results of sample HK25600, which yields T > 700°C. The amphibole-involving equilibria are affected in *P* to a somewhat greater extent since a shift in pressure of > 0.3 GPa occurs when using *average P-T* calculations involving amphiboles (M2-H_2O+Amph). Again, similar to the multi-equilibrium calculations of the amphibolites as shown above, this shift in pressure is mostly due to decreasing pargasite and increasing tremolite activities due to changes in the amphibole *a-X* relations from THERMOCALC v.3.21 (*AX* 2000; model of Dale et al., 2000) to THERMOCALC v.3.33 (*AX* 2008; model of Dale et al., 2005). With respect to previously obtained *P-T* estimates using multi-equilibrium- and pseudosection calculations (Tribus et al., 2008; Miladinova et al., 2022), the amphibole-absent *P-T* results using THERMOCALC v.3.21 and v.3.33 are in much better agreement than the amphibole-involving results, since latter show higher *T* of 640–740°C.

5.2.2 Zr-in-rutile and Zr-in-titanite geothermometry

Zirconium-in-rutile geothermometry of eclogite sample HK25600 using the calibration of Ferry and Watson (2007) yields temperatures of 580 to 640°C. Zirconium-in-titanite geothermometry using the calibration of Hayden et al. (2008) was applied to titanite rims that formed around rutile, supposedly later than rutile crystallization. This geothermometer also needs constraints on the values of *a*SiO2 and *a*TiO2. Since quartz and rutile coexist with titanite it is reasonable to assume both values to be 1. On the other hand, pressure plays an important role since the calculation assuming pressures of 2 GPa yield unrealistically high temperatures of 750–850°C for titanite formation at the rim of rutile. In order to obtain temperature values consistent with zirconium-in-rutile geothermometry the pressure needs to be lower than 0.5 GPa, indicating that titanite grew around rutile at low pressures, thus being part of a later-stage retrograde greenschist/amphibolite-facies assemblage as indicated by Habler et al. (2006). Temperatures calculated at 0.5 GPa range at 600–630°C, which are considered as an upper temperature limit.

6. Discussion

Geothermobarometric investigations of the Texel Unit eclogites have evolved over the years from using simple phase equilibria to constrain the metamorphic peak *P-T* conditions to complex calculations utilizing phase equilibria or thermodynamically stable mineral assemblages involving internally-consistent databases. One characteristic feature occurred over the years: while earlier only limiting pressure estimates could be obtained, calculations using a multitude of phases and reactions later yield increased pressure estimates. A very characteristic example is the Texel Unit. Initially Hoinkes et al. (1991) obtained limiting pressures of 1.1 to 1.2 GPa using the breakdown of albite to jadeite + quartz. Then Habler et al. (2006) also used this albite-breakdown reaction assuming plagioclase in equilibrium with omphacite and obtained slightly higher pressures of 1.2 to 1.4 GPa. Zanchetta et al. (2013) used conventional geothermobarometry and obtained extremely high *P-T* conditions of 2.65–2.90 GPa and 630–690°C (Fig. 6).

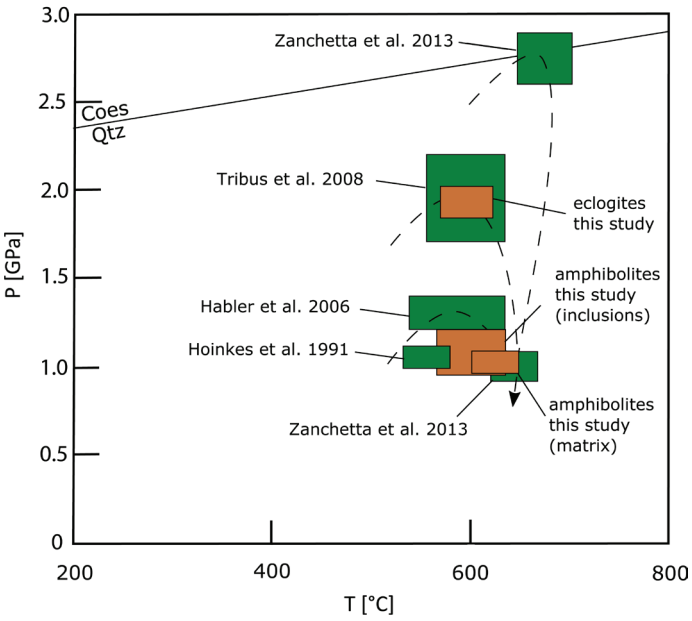

Figure 6: Geothermobarometric results of the eclogites showing the results of Habler et al. (2006); Tribus et al. (2008) and Zanchetta et al. (2013) as green boxes. The results of this study are shown in light brown boxes. The *P-T* conditions of the eclogites are based on using mode-1 (M1-H_2O-Amph) and average *P-T* mode-2 (M2-H_2O-Amph) calculations. Coes = coesite; Qtz = quartz.

The eclogite samples of this study derive from outcrops of the Texel Unit in the Saltaus valley (Habler et al., 2006) and yield overall *P-T* results of 590–680°C and 1.7–2.3 GPa (Tab. 3). The higher *T* results are due to the addition of new phase components (ferroceladonite) and amphiboles to the calculations. Although there is textural evidence that the amphiboles are part of the eclogite-facies assemblage, because of the uncertainties with respect to the use of different amphibole activity models we consider the calculations without H_2O and amphiboles (M1-H_2O-Amph, M2-H_2O-Amph) to be the most robust results. These calculations yield mean temperatures of 580–600°C at a mean pressure of 1.9–2 GPa (Tab. 3, Fig. 6). In contrast to the *P-T* data of Habler et al. (2006) of

550–600°C and 1.2–1.4 GPa the obtained *P-T* conditions are significantly higher with respect to *P* but agree with *P* obtained by Tribus et al. (2008) and Miladinova et al. (2022). Tribus et al. (2008) used multi-equilibrium calculations with THERMOCALC v.3.21 and yield higher *P-T* conditions of 1.8–2.2 GPa and 560–600°C. These calculations involved the mineral assemblage garnet + omphacite + epidote + quartz and garnet + omphacite + Na-Ca amphibole + epidote + quartz. Their study also has shown, that the obtained *P-T* results are strongly dependent on aH_2O and on the choice of the amphibole activity models. Recently Miladinova et al. (2022) used pseudosection geothermobarometry (intersecting compositional isopleths of garnet) with the software Theriak-Domino (de Capitani and Petrakakis, 2010) and obtained *P-T* conditions of 570–600°C and 1.9–2.1 GPa. Both investigations do not confirm the UHP conditions of Zanchetta et al. (2013) from the eclogites in the Ulfas valley, who obtained *P-T* conditions of 2.65–2.90 GPa and 630–690°C with estimated errors of ±0.20 GPa and ±50 °C. They used conventional geothermobarometry since the *P-T* estimates of the eclogite-facies assemblage (M1) were obtained with the garnet-phengite (Green and Hellman, 1982) and garnet-clinopyroxene (Krogh-Ravna, 2000) Fe-Mg exchange geothermometers, and the garnet-phengite-clinopyroxene geobarometer (Waters and Martin, 1993. The problem with the approach of Zanchetta et al. (2013) lies (1) in the inconsistency of the thermodynamic data since data from an internally consistent database were combined with data from internally non-consistent sources and (2) the use of an outdated garnet activity model for the garnet-phengite-clinopyroxene geobarometer such as the activity model of Newton and Haselton (1981). (3) in addition, this approach does not allow for a reliable error propagation of the results.

Calculation of *P-T* conditions of eclogites is challenging since the results strongly depend on the choice of thermodynamic data and activity models. Tropper (2014) recalculated one sample (1396B) of the M1 assemblage garnet + omphacite + phengite + zoisite + quartz of Zanchetta et al. (2013) to illustrate the influence of thermodynamic parameters on the results. The calculations by Tropper (2014) were done using the garnet-phengite-clinopyroxene geobarometer (Waters and Martin, 1993; Krogh-Ravna and Terry, 2004), THERMOCALC v.3.21 and THERMOCALC v.3.33 (*average P-T* mode-2) and the calculations yield a wide spread in *P-T* data (just for illustration purposes, no errors are given): the garnet-phengite-clinopyroxene geobarometer calibration by Waters and Martin (1993; dataset: Holland and Powell, 1990) gave 650°C and 2.55 GPa, the garnet-phengite-clinopyroxene geobarometer calibration by Krogh-Ravna and Terry (2004; dataset Holland and Powell, 1998) yield 740°C and 4.2 GPa. Multi-equilibrium calculations using THERMOCALC v.3.21 resulted in 650°C and 2.9 GPa, and using THERMOCALC v.3.33 yield 610°C and 2.75 GPa. When looking at the change in garnet phase component activities as a function of *P* and *T* the calculations yield a systematic increase of the activities of grossular and pyrope with pressure. These changes are also associated with the choice of the garnet activity model. The calibration of Waters and Martin (1993) uses the simple activity model of Newton and Haselton (1981) which considers only the WMg-Ca interaction parameter in a garnet solid solution, whereas the calibration of Krogh-Ravna and Terry (2004) uses the quaternary activity model of Ganguly et al. (1996) and both THERMOCALC v.3.21 and v.3.33 programs also use a quaternary activity model based on their internally consistent database. Nonetheless, despite the differences in the thermodynamic databases and activity models, the obtained *P-T* conditions are valid estimates but *P* conditions > 2.5 GPa still very high when compared with *P* estimates from this study.

Our geothermobarometric results from this study are in agreement with previous *P-T* estimates from eclogites of the Eoalpine high-pressure belt such as the Schober and Kreuzeck Group: 630–690°C and 1.6–1.8 GPa (Linner, 1999; Hauke et al. 2022); the Saualpe 700–740°C and 2.2–2.5 GPa (Miller et al., 2005) and the Koralpe Complex: 600–650°C and 1.8–2.0 GPa (Miller and Thöni, 1997; Herg and Stüwe, 2018); but still lower than maximum *P-T* condition of 3–3.1 GPa and 760–825°C proposed for Pohorje (Janak et al., 2004; Sassi et al., 2004; Herg and Stüwe, 2018).

The amphibolites from Spronsertal represent a distinct Eoalpine *P*-accentuated metamorphic event. Based on the chemical zonation of the amphiboles it is possible to reconstruct part of the *P-T* evolution, where the *T* maximum is reached after the pressure maximum (Fig. 6). This is evident by amphibole analyses from core and rim (R1+R2 and R3) which show decreasing glaucophane component from the core to the rims, indicating slightly higher *P* conditions during formation of the cores compared to the rim. Furthermore, increasing edenite component from core to rim points to slightly higher *T* conditions during amphibole rim formation. This is indicative of a typical *P-T* path associated with continental collision. The obtained *P-T* conditions of this *P*-accentuated amphibolite-facies metamorphic overprint of 550–650°C and 0.8–1.3 GPa for the garnet inclusion assemblage are slightly higher in *P* and lower in *T* than the *P-T* conditions of the amphibolite matrix assemblage, which yield 600–650°C and 1–1.1 GPa (Fig. 6). Since the amphibole cores are katophoritic in composition, similar to the amphiboles in the eclogites, and the *P-T* conditions of the garnet inclusion assemblage yield slightly higher *P,* these amphibolites may likely represent former eclogites that fully-equilibrated under *P*-accentuated amphibolite-facies conditions. The matrix *P-T* data are in excellent agreement with *P-T* data from metapelites from the Ziel valley (Pomella et al., 2016) and amphibolites from the Ulfas valley (Zanchetta et al., 2013). Flöss (2009) obtained 580–660°C and 0.9–1.2 GPa using conventional- as well as multi-equilibrium geothermobarometry. According to Zanchetta et al. (2013) the full amphibolite facies re-equilibration of eclogites corresponding to the forma-

tion of amphibole-plagioclase coronae around garnet, occurred at *P-T* conditions of 610–650°C and 0.9–1.1 GPa, as derived from application of the geothermobarometers by Dale et al. (2000). These *P*-accentuated Eoalpine *P-T* conditions following the eclogite-facies stage (ca. 95–80 Ma; Sölva et al., 2005; Habler et al., 2006; Zanchetta et al., 2013) are also observed in garnet amphibolites and retrograde eclogites from the Kreuzeck group (Polinik Unit) where 600°C and 1.0–1.4 GPa were obtained (Hoke, 1990), as well as the Wölz Unit and the Millstatt Unit with *P-T* conditions of 600°C and 1.0 GPa (Schuster and Frank, 1999) and the Schobergruppe (Hauke et al., 2019).

7. Conclusions

The eclogites of the Eoalpine High Pressure Belt represent the remnants of intracontinental subduction of crustal materials in an intracontinental shear zone (Schmid et al., 2004). The NW-SE directed change in peak pressure of Eoalpine metamorphism of 1.8 to > 3 GPa across the Eastern Alps can be observed in the Austroalpine units to the west, south and the east of the Tauern Window. In contrast to the *P-T* data of Habler et al. (2006) of 550–600°C and 1.2–1.4 GPa the obtained *P-T* conditions of the westernmost eclogites of the EHB from this study are significantly higher with respect to *P* (1.9–2 GPa) but similar with respect to *T* (580–600°C). Our data agree with recent *P-T* estimates obtained by Miladinova et al. (2022). The Saltaus eclogites reflect the Eoalpine intracontinental subduction stage at ca. 2 GPa. The retrogression of the eclogites and the re-equilibration to amphibolites reflect the subsequent, *P*-accentuated, stage of Eoalpine decompression (1–1.2 GPa and 600–650°C) during exhumation within the shear zone associated with the subsequent Eoalpine collisional stage followed then by a Late Cretaceous extension (Ducan Ela Phase after Froitzheim et al., 1994).

Acknowledgements

Bernhard Sartory is thanked for his help with electron probe microanalysis. The journal reviewers Bernhard Schulz and Irina Miladinova are thanked for their concise comments and Kurt Stüwe is thanked for his thorough editorial handling and his comments, all helped to improve the manuscript considerably.

References

Bargossi, G.M., et al., 2010. Erläuterungen zur geologischen Karte von Italien im Maßstab 1:50 000 Blatt 013 Meran, CARG. ISPRA, Istituto Superiore per la Protezione e la Ricerca Ambientale, SystemCart Roma, p. 320.

Dachs, E., 1998. PET: petrological elementary tools for Mathematica. Computers and Geosciences, 243, 219–235.

Dale, J., Holland, T.J.B., Powell, R., 2000. Hornblende-garnet-plagioclase thermobarometry: a natural assemblage calibration of the thermodynamics of hornblende. Contributions to Mineralogy and Petrology, 140, 353–362.

Dale, J., Powell, R., White, R. W., Elmer, F. L., Holland, T.J.B., 2005. A thermodynamic model for Ca-Na clinoamphiboles in Na_2O-CaO-FeO-MgO-Al_2O_3-SiO_2-H_2O-O for petrological calculations. Journal of Metamorphic Geology, 238, 771–791.

de Capitani, C., Petrakakis, K., 2010. The computation of equilibrium assemblage diagrams with Theriak/Domino software. American Mineralogist, 957, 1006–1016.

Eisbacher, G. H., Linzer, H. G., Meier, L., Polinski, R., 1990. A depth-extrapolated structural transect across the Northern Calcareous Alps of western Tirol. Eclogae Geologicae Helvetiae, 83, 711–725.

Ferry, J.M., Watson, E.B., 2007. New thermodynamic models and revised calibrations for the Ti in-zircon and Zr-in-rutile thermometers. Contributions to Mineralogy and Petrology, 154, 429–437.

Flöss, D., 2009. Tektonometamorphe Entwicklung der westlichen Austroalpinen Einheiten: Geometrie und Kinematik der eoalpinen Kollision (Texel Komplex, Südtirol). Unpublished Diploma Thesis, University of Innsbruck, p. 133.

Froitzheim, N., Schmid. S.M., Conti, P., 1994. Repeated change from crustal shortening to orogen-parallel extension in the Austroalpine units of Graubünden. Eclogae Geologicae Helvetiae, 87, 559–612.

Froitzheim, N., Conti, P., van Daalen, M., 1997. Late Cretaceous, synorogenic, low-angle normal faulting along the Schlinig fault Switzerland, Italy, Austria and its significance for the tectonics of the Eastern Alps. Tectonophysics, 280, 267–293.

Fügenschuh, B., 1995. Thermal and kinematic history of the Brenner area Eastern Alps, Tyrol. Unpublished Doctoral Dissertation, ETH Zurich, p. 225.

Ganguly, J., Cheng, W., Tirone, M., 1996. Thermodynamics of aluminosilicate garnet solid solution: new experimental data, an optimized model, and thermometric applications. Contributions to Mineralogy and Petrology, 126, 137–151.

Green, T.H., Hellman, P.L., 1982. Fe-Mg partitioning between coexisting garnet and phengite at high pressure, and comments on a garnet-phengite geothermometer. Lithos, 154, 253–266.

Habler, G., Thöni, M., Sölva, H., 2006. Tracing the high-pressure stage in the polymetamorphic Texel Complex Austroalpine basement unit, Eastern Alps P-T-t-d constraints. Mineralogy and Petrology, 88, 269–296.

Hauke, M., Froitzheim, N., Nagel, T. J., Miladinova, I., Fassmer, K., Fonseca, R.O.C., Sprung, P., Münker, C., 2019. Two high-pressure metamorphic events, Variscan and Alpine, dated by Lu-Hf in an eclogite complex of the Austroalpine nappes Schobergruppe, Austria. International Journal of Earth Sciences.

Hayden, L.A., Watson, E.B., Wark, D.A., 2008. A thermobarometer for sphene titanite. Contributions to Mineralogy and Petrology, 155, 529–540.

Herg, A., Stüwe, K., 2018. Tectonic interpretation of the metamorphic field gradient south of the Koralpe in the Eastern Alps. Austrian Journal of Earth Sciences, 111, 155–170.

Hoinkes, G., Kostner, A., Thöni, M., 1991. Petrological constraints for Eoalpine eclogite-facies metamorphism in the Austroalpine Ötztal Basement. Mineralogy and Petrology, 43, 237–254.

Hoinkes, G., Koller, F., Rantitsch, G., Dachs, E., Höck, V., Neubauer, F., Schuster, R., 1999. Alpine metamorphism of the Eastern Alps. Schweizerische Mineralogische und Petrographische Mitteilungen 79, 155–181.

Hoke, L., 1990. The Altkristallin of the Kreuzeck Mountains, SE Tauern Window, Eastern Alps - Basement crust in a convergent plate boundary zone. Jahrbuch der Geologischen Bundesanstalt, 133, 5–87.

Holland, T.J.B., Powell, R., 1998. An internally consistent thermodynamic data set for phases of petrological interest. Journal of. Metamorphic Geology, 16, 309–343.

Janák, M., Froitzheim, N., Lupták, B., Vrabec, M., Krogh Ravna, E.J., 2004. First evidence for ultrahigh-pressure metamorphism of Eclogites in Pohorje, Slovenia: Tracing deep continental subduction in the eastern Alps. Tectonics, 23.

Klotz, T., Pomella, H., Reiser, M., Fügenschuh, B., Zattin, M., 2019. Differential uplift on the boundary between the Eastern and the Southern European Alps: Thermochronologic constraints from the Brenner Base Tunnel. Terra Nova, 31, 281–294.

Klug, L., Froitzheim, N., 2022. Reuniting the Ötztal Nappe: the tectonic evolution of the Schneeberg Complex. International Journal of Earth Sciences, 1112, 525–542.
Krenn, K., Kurz, W., Fritz, H., Hoinkes, G., 2011. Eoalpine tectonics of the Eastern Alps: implications from the evolution of monometamorphic Austroalpine units Schneeberg and Radenthein Complex. Swiss Journal of Geosciences, 104, 471–491.
Krogh Ravna, E.J., Terry, M.P., 2004. Geothermobarometry of UHP and HP eclogites and schists-an evaluation of equilibria among garnet-clinopyroxene-kyanite-phengite-coesite/quartz. Journal of Metamorphic Geology, 226, 579–592.
Leake, B.E., et al., 1997. Nomenclature of amphiboles: Report of the Subcommittee in amphiboles of the International Mineralogical Association, Commission on New Minerals and Mineral Names. American Mineralogist, 82, 1019–1037.
Linner, M., 1999. Die P-T-t Entwicklung der Eklogite im Schoberkristallin als Beleg für frühalpidische kontinentale Subduktion im Ostalpinen Kristallin. Unpublished Doctoral Dissertation University of Vienna, p. 167.
Mancktelow, N.S., Stöckli, D.F., Grollimund, B., Müller, W., Fügenschuh, B., Viola, G., Seward, D., Villa, I.M., 2001. The DAV and Periadriatic fault systems in the Eastern Alps south of the Tauern window. International Journal of Earth Sciences, 90, 593–622.
Miladinova, I., Froitzheim, N., Nagel, T.J., Janak, M., Fonseca, R.O., Sprung, P., Münker, C., 2022. Constraining the process of intracontinental subduction in the Austroalpine Nappes: Implications from petrology and Lu-Hf geochronology of eclogites. Journal of Metamorphic Geology, 403, 423–456.
Miller, C., Thöni, M., 1997. Eoalpine eclogitisation of Permian MORB-type gabbros in the Koralpe Eastern Alps, Austria: new geochronological, geochemical and petrological data. Chemical Geology, 137, 283–310.
Miller, C., Thöni, M., Konzett, J., Kurz, W., Schuster, R., 2005. Eclogites from the Koralpe and Saualpe type-localities; Eastern Alps, Austria. Mitteilungen der Österreichischen Mineralogischen Gesellschaft, 150, 227–263.
Mogessie, A., Ettinger, K., Leake, B.E., Tessadri, R., 2001. AMPH-IMA97: a hypercard program to determine the name of an amphibole from electron microprobe and wet chemical analyses. Computers and Geosciences, 27, 1169–1178.
Montemagni, C., Zanchetta, S., Rocca, M., Villa, I.M., Morelli, C., Mair, V., Zanchi, A., 2023. Kinematics and time-resolved evolution of the main thrust-sense shear zone in the Eo-Alpine orogenic wedge (the Vinschgau Shear Zone, eastern Alps). Solid Earth, 14/5, 551–570.
Newton, R.C., Haselton, H.T., 1981. Thermodynamics of the garnet-plagioclaseAl2SiO5-quartz geobarometer. Thermodynamics of Minerals and Melts, 131–147.
Oberhänsli, R. (ed.), 2004. Explanatory Notes to the Map Metamorphic Structure of the Alps. Mitteilungen der Österreichischen Mineralogischen Gesellschaft, 149, 115–226.
Poli, S., 1991. Reaction spaces and PT paths: from amphibole eclogite to greenschist facies in the Austroalpine domain Ötztal Complex. Contributions to Mineralogy and Petrology, 1064, 399–416.
Pomella, H., Flöss, D., Speckbacher, R., Tropper P., Fügenschuh, B., 2016. The western end of the Eoalpine High-Pressure Belt Texel unit, South Tyrol/Italy. Terra Nova, 28, 60–69.
Pomella, H., Costantini, D., Aichholzer, P., Reiser, M., Schuster, R., Tropper, P., 2022. Petrological and geochronological investigations on the individual nappes of the Meran-Mauls nappe stack Austroalpine unit/South Tyrol, Italy. Austrian Journal of Earth Sciences, 115, 15–40.
Powell, R., Holland, T.J.B., 2008. On thermobarometry. Journal of Metamorphic Geology, 26, 155–179.
Ravna, K., 2000. The garnet-clinopyroxene Fe2+-Mg geothermometer: an updated calibration. Journal of Metamorphic Geology, 182, 211–219.
Sassi, R., Mazzoli, C., Miller, C., Konzett, J., 2004. Geochemistry and metamorphic evolution of the Pohorje Mountain eclogites from the easternmost Austroalpine basement of the Eastern Alps Northern Slovenia. Lithos, 783, 235–261.
Schmid, S.M., Fügenschuh, B., Kissling, E., Schuster, R., 2004. Tectonic map and overall architecture of the Alpine orogen. Eclogae Geologicae Helvetiae, 97, 93–117.
Schuster, R., Frank W., 1999. Metamorphic evolution of the Austroalpine units east of the Tauern window: indications for Jurassic strike slip tectonics. Mitteilungen der Gesellschaft für Geologie und Bergbaustudenten Österreichs, 42, 37–58.
Sölva, H., Thöni, M., Grasemann, B., Linner, M., 2001. Emplacement of Eoalpine high-pressure rocks in the Austroalpine Ötztal complex Texel group, Italy/Austria. Geodinamica Acta, 14, 345–360.
Sölva, H., Grasemann, B., Thöni, M., Thiede, R.C., Habler, G., 2005. The Schneeberg Normal Fault Zone: Normal faulting associated with Cretaceous SE-directed extrusion in the Eastern Alps Italy, Austria. Tectonophysics, 401, 143–166.
Spalla, M.I., 1993. Microstructural control on the PT path construction in metapelites from the Austroalpine crust Texel Gruppe, Eastern Alps. Schweizerische Mineralogische und Petrographische Mitteilungen, 73, 259–275.
Thöni, M., Jagoutz, E., 1993. Isotopic constraints for Eoalpine high-P metamorphism in the Austroalpine nappes of the Eastern Alps: bearing on Alpine orogenesis. Schweizerische Mineralogische und Petrographische Mitteilungen, 73, 177–189.
Thöni, M., 2006. Dating eclogite-facies metamorphism in the Eastern Alps - approaches, results, interpretations: a review. Mineralogy and Petrology, 88, 123–148.
Tribus, M., Tropper, P., Habler, G., 2008. Multi-equilibrium thermobarometry of eclogites from the Texel Complex South-Tyrol, Italy. Journal of Alpine Geology, 49, 223–224.
Tribus, M., 2008. Petrologische und termobarometrische Untersuchungen des amphibolit/eklogitfaziellen eo-Alpinen Events in den Metabasiten des Texel Komplexes. Unpublished Diploma Thesis, University of Innsbruck, p. 110.
Tropper, P., 2014: P,T = f(t): geothermobarometry of eclogites as a function of time, or the phenomenon of increasing pressures over the years. In: Berichte des Instituts für Erdwissenschaften der Karl-Franzens-Universität Graz 20/1, 211.
Viola, G., Mancktelow, N., Seward, D., Meier, A., Martin, S., 2003. The Pejo fault system: An example of multiple tectonic activity in the Italian Eastern Alps. Geological Society of America Bulletin 115, 515–532.
Viola, G., Mancktelow, N.S., Seward, D., 2001. Late Oligocene-Neogene evolution of Europe-Adria collision: New structural and geochronological evidence from the Giudicarie fault system Italian Eastern Alps. Tectonics 20, 999–1020.
Waters, D., Martin, H.N., 1993. The garnet-clinopyroxene-phengite barometer. Terra Abstracts 5, 410–411.
Zanchetta, S., Poli, S., Rubatto, D., Zanchi, A., Bove, G., 2013. Evidence for deep subduction of Austroalpine crust Texel Complex, NE Italy. Rendiconti Lincei, 24, 163–176.
http://geokatalog.buergernetz.bz.it. Online platform of geodata, Autonomous Province of Bozen/Bolzano (Italy).

Received: 11.4.2023
Accepted: 25.11.2023
Editorial Handling: Kurt Stüwe